Video Article

Photoacoustic Cystography

Mansik Jeon[1,2], Jeehyun Kim[3], Chulhong Kim[1,2]

[1]Department of Biomedical Engineering, University at Buffalo, The State University of New York

[2]Department of Creative IT Engineering, Pohang University of Science and Technology (POSTECH)

[3]School of Electrical Engineering and Computer Science, Kyungpook National University

Correspondence to: Chulhong Kim at chulhong@postech.edu

URL: http://www.jove.com/video/50340
DOI: doi:10.3791/50340

Keywords: Biomedical Engineering, Issue 76, Biophysics, Medicine, Bioengineering, Cancer Biology, Engineering (General), Electronics and Electrical Engineering, Lasers and Masers, Acoustics, Optics, Photoacoustic cystography, nonionizing imaging, contrast agent, urinary tract reflux, bladder, cystography, photoacoustic tomography, PAT, tomography, imaging, clinical techniques, animal model

Date Published: 6/11/2013

Citation: Jeon, M., Kim, J., Kim, C. Photoacoustic Cystography. *J. Vis. Exp.* (76), e50340, doi:10.3791/50340 (2013).

Abstract

Conventional pediatric cystography, which is based on diagnostic X-ray using a radio-opaque dye, suffers from the use of harmful ionizing radiation. The risk of bladder cancers in children due to radiation exposure is more significant than many other cancers. Here we demonstrate the feasibility of nonionizing and noninvasive photoacoustic (PA) imaging of urinary bladders, referred to as photoacoustic cystography (PAC), using near-infrared (NIR) optical absorbents (*i.e.* methylene blue, plasmonic gold nanostructures, or single walled carbon nanotubes) as an optical-turbid tracer. We have successfully imaged a rat bladder filled with the optical absorbing agents using a dark-field confocal PAC system. After transurethral injection of the contrast agents, the rat's bladders were photoacoustically visualized by achieving significant PA signal enhancement. The accumulation was validated by spectroscopic PA imaging. Further, by using only a laser pulse energy of less than 1 mJ/cm^2 (1/20 of the safety limit), our current imaging system could map the methylene-blue-filled-rat-bladder at the depth of beyond 1 cm in biological tissues *in vivo*. Both *in vivo* and *ex vivo* PA imaging results validate that the contrast agents were naturally excreted via urination. Thus, there is no concern regarding long-term toxic agent accumulation, which will facilitate clinical translation.

Video Link

The video component of this article can be found at http://www.jove.com/video/50340/

Introduction

X-ray cystography[1] is an imaging process to identify bladder-related diseases such as bladder cancer, vesicoureteral reflux, blockage of ureters, neurogenic bladder, *etc.*[2-5] Typically, urines are voided and a radio-opaque agent is injected through a catheter. Then, fluoroscopic X-ray images are acquired to delineate urinary bladders. However, the key safety issue is that harmful ionizing radiation is used in this procedure. The percentage of cumulative cancer risk to age 75 years owing to diagnostic X-rays ranges from 0.6 to 1.8%.[6] In addition, the carcinogenic threat is significant in pediatric patients. A UK study showed that among 9 major internal organs, the average annual radiation dose from diagnostic X-rays was highest in the bladders in female children less than 4 and second highest in male children less than 4.[7] This indicates that the bladder cancer risk is most significant in pediatric patients. Although pediatric radiologists endeavor to reduce the radiation exposure rate as low as reasonably achievable, ionizing radiation cannot be completely excluded. Therefore, the limitation creates a need for a completely radiation-free, sensitive, cost-effective, and high-resolution imaging modality with nonradioactive contrast agents in cystography.

Recently, photoacoustic tomography (PAT) has become a premier biomedical imaging modality because PAT can provide strong optical absorption contrasts and a high ultrasonic spatial resolution in biological tissues.[8] The principle of PAT is that ultrasonic waves are induced due to thermoelastic expansion of a target followed by light absorption. By detecting time-resolved acoustic waves travelling *via* a medium, two- or three-dimensional photoacoustic (PA) images are formed. Because ultrasound (US) is much less scattered in tissues compared to light (typically two or three orders of magnitude), the imaging depth of PAT can reach up to ~8 cm in tissues, while the spatial resolution is maintained to 1/200 of the imaging depth.[9] The key advantages of PAT for the cystographic application include: (1) PAT is completely free from ionizing radiation. (2) ClinicalUSimaging systems can be easily adapted to supply dual-modal PA and US imaging capabilities. Thus, the dual-modal PA/US imaging system can be relatively portable, cost-effective, and fast, which are key criteria for fast clinical translation. Using both endogenous and exogenous contrasts, PAT has provided high-resolution morphological, functional, and molecular imaging of tissues to study tumor physiopathology, brain hemodynamics, internal organs, ophthalmology, angiography, and *etc.* [10-16]

In this article, we demonstrate the experimental protocols of nonionizing photoacoustic cystography (PAC) using near-infrared (NIR) optical absorbents (*i.e.* methylene blue, gold nanocages, or single walled carbon nanotubes) as nontoxic optical-turbid tracers. Rat bladders filled with the contrast agents were photoacoustically and spectroscopically delineated *in vivo*. No agents persistently accumulated in the bladders and kidneys of the rats. Thus, long-term toxicity which may be caused by agent accumulation can be excluded. This result implies that PAC with combination of the optical absorbers can potentially be a truly harmless cystographic modality for pediatric patients. The system configuration, system alignment, and *in vivo* / *ex vivo* imaging procedures are discussed in this article.

Protocol

1. Deep Reflection Mode Photoacoustic Cystography (PAC) System

1. System configuration[17, 18]
    1. A Q-switched Nd:YAG laser (SLII-10; Continuum; 532 nm) pumps a wavelength-tunable laser (Surelite OPO PLUS; Continuum; wavelength tuning range: 680 to 2,500 nm).
    2. The pulse duration of each laser shot is ~5 nsec, and the laser repetition rate is 10 Hz.
    3. The wavelength depends on the optical absorption peak of the used contrast agent. If methylene blue serves as the contrast agent, an optical wavelength of 667 nm is used, where the peak absorption is. Plasmonic gold nanostructures can have tunable localized surface plasmon resonance at the NIR spectral region, based on their physical and chemical properties. Further, the broad absorption spectrum of single walled carbon nanotubes can provide a wide option for wavelength selection.
    4. Light coming out of the tunable laser is delivered to a spherical conical lens through right angle prisms (PS908, Thorlabs).
    5. A donut-shaped light beam pattern is generated after the light passes through the spherical conical lens. The home-made conical lens is made from a BK7 lens and the cone angle is 152°. The diameter of the lens is 2.5 cm.
    6. The diverging donut-shaped light beam is redirected *via* an optical condenser, made of a transparent acrylic sheet. The diameters of the top and bottom surfaces are 6.1 and 4.8 cm, respectively. The thickness of the condenser is 2.5 cm. The redirected ring-shaped light beam forms a donut-shaped with a dark center on the tissue surface.
    7. Utilize a small water container to boost acoustic coupling. The water container has a bottom opening wrapped with a clear thin polyethylene film which is optically and acoustically transparent. Small animals are positioned under the water container.
    8. The generated PA waves are detected by a spherically focused ultrasound transducer (V308; Olympus NDT; 5 MHz central frequency), which is mounted in the middle of the optical condenser. The element diameter and focal length of the transducer are 1.9 and 2.5 cm, respectively. Thus, the f-number of the transducer is ~1.3.
    9. The transverse and axial resolutions are 590 and 144 µm, respectively.
    10. The detected PA waves are first amplified by a broadband ultrasonic pulser/receiver (5072PR; Olympus NDT; 35 MHz bandwidth and 59 dB rf gain), and then acquired by an oscilloscope (TDS5054; Tektronix).
    11. Obtain one-dimensional time-resolved images (called as A-line) by measuring the times of arrival of the PA waves. Currently, the speed of PA waves is assumed to be at 1,480 m/sec over the entire image acquisition. Two- (called as B-scans) and three-dimensional PA images can be acquired by mechanically moving the linear raster scanning stage (XY6060; Danaher Dover).
    12. The imaging time is ~25 min for one volumetric single-wavelength PA image with a field of view (FOV) of 2.5 x 2.4x 1.5 cm^3 in the x-y-z planes. We acquired 125 samples along the x direction with a step size of 0.2 mm, 60 samples along the y direction with a step size of 0.4 mm. 500 data points with a 50-MHz sampling rate were obtained along the z direction. The mechanical scanning is controlled by a home-made NI LabVIEW software system.
    13. The volumetric data is represented by maximum amplitude projection (MAP) using a MathWorks MATLAB software system.

2. System alignment
    1. After the spherical conical lens, make sure that the beam pattern is a perfect ring shape. If the donut-shaped beam pattern is not properly generated, the PA signals originated from the skin surface are dominant. Thus, it is difficult to achieve deep tissue imaging.
    2. The line-shaped light focus in water should be coaxially aligned with the ultrasound focal zone. If those are not coaxially aligned, the system suffers from low signal-to-noise ratio.
    3. The irradiated laser pulse energy on the skin surface is varied from ~1 - 2 mJ/cm^2 when the wavelength is tuned from 680 to 1,000 nm, respectively. These laser pulse energies are much lower than the American National Standards Institute safety limit, varying from 20 to 80 mJ/cm^2 over the spectral region, respectively.

2. *In vivo* and *Ex vivo* Imaging Procedures

1. Animal preparation
    1. Use female Spraque-Dawley rats with a weight of 200 - 250 g in all PA imaging experiments.
    2. To begin with, anesthetize the rat by intraperitoneal injection of a mixture of ketamine (85 mg/kg of body weight) and xylazine (15 mg/kg).
    3. Depilate the hairs in the abdominal area.
    4. Position the rat atop of a custom-made animal holder.
    5. Coat a 22-gauge catheter with lubricant to improve the catheter insertion.
    6. Hold the catheter vertically over the urethral opening. Next, insert the distal end of the catheter, horizontally, into the urethra until the hub of the catheter finally reaches the opening.
    7. Urine in the bladder will void via the catheter.

2. *In vivo* PAC imaging
    1. Position the rat, located on top of the animal holder, below the water container in the PAC system.
    2. Apply ultrasound gel (Sonotech) between the animal skin surface and plastic membrane to improve acoustic coupling.
    3. Fully anesthetize the rat using vaporized isoflurane (1 L/min of oxygen and 0.75% isoflurane) during the *in vivo* PA imaging experiments.
    4. Obtain a control PA image prior to injection of contrast agents.
    5. Introduce an aqueous solution of methylene blue (0.8 µl/g body weight with a concentration of 30 mM), gold nanocages (1.2 µl/g body weight with a concentration of 2 nM), or single walled carbon nanotubes (0.8 µl/g body weight with a concentration of 0.3 µM) to the bladder *via* the catheter. Use a 1-ml-syringe with a 22-gauge catheter.

6. Acquire a series of PA images.

3. *Ex vivo* PAC imaging
   1. Sacrifice the rat after *in vivo* PAC imaging, by injecting an overdose of pentobarbital.
   2. Remove the two major organs, bladders and kidneys, to investigate biodistribution, and on a glass plate.
   3. Position the glass plate below the water container in the PAC system.
   4. Apply ultrasound gel (Sonotech) between the excised organs and plastic membrane to improve acoustic coupling.
   5. Acquire PA images.
   6. Photoacoustically image the organs removed from a healthy rat as a control.

Representative Results

Figure 1 shows the *In vivo* nonionizing and noninvasive PAC using optically turbid methylene blue (MB). The control PA image was obtained at 667 nm, at the peak optical absorption for MB (**Figure 1A**). Although the blood vessels in the FOV are clearly visualized, the bladder is invisible because it is optically transparent at this wavelength. As shown in **Figure 1B**, the bladder is clearly revealed in the PA image acquired at 0.2 hr post-injection of MB. To confirm the accumulation of MB in the bladder, we used two optical wavelengths (667 and 850 nm) to distinguish between the bladder filled with MB from the surrounding structures. As shown in **Figure 1C**, the PA amplitudes within the bladder are not visible because the optical absorption coefficient of MB at 850 nm is nearly 0. Thus, this result indicates that the bladder is filled with MB. As a result, it demonstrates that the spectroscopic PA image can clearly distinguish different endogenous and exogenous choromophores. **Figures 1D** and **1E** show the depth-resolved PA B-scan images, scanned along the dotted line in **Figures 1A** and **1B**, respectively. The top surface of the bladder was located at the ultrasound transducer focal point both *in vivo* and *ex vivo* imaging. The position of the bladder along the depth direction is clearly identified, ~3.5 mm below the skin surface. In addition, the PA signals within the bladder measured at 24 and 48 hr post-injection are almost identical to the signal obtained at pre-injection. This result implies that the injected contrast agent was completely removed from the body, and no agent accumulated. Therefore, no long-term agent toxicity is expected in our approach. Moreover, the depth of the post-injection PA image (**Figure 1B**) is encoded using a pseudo color in **Figure 2**. The position of the bladder is ~3.5 mm below the skin surface, which correlates well with the depth-resolved PA B-scan image (**Figure 1E**). The typical depths of the top and bottom boundaries of a pediatric bladder are ~1.4 and 4.3 cm, respectively, from the abdominal surface. By using only a laser pulse energy of less than 1 mJ/cm^2 (1/20 of the safety limit), our current imaging system could map the methylene-blue-filled-rat-bladder at the depth of beyond 1 cm in biological tissues *in vivo*.[17] As we above mentioned, the imaging depth of PAT can reach up to ~8 cm in tissues with aid of methylene blue.[9]

After all *in vivo* imaging experiments, we excised two major organs, bladder and kidney to investigate biodistribution. As a control, a bladder and kidney were excised from a healthy rat. The PA signals measured within the removed bladders and kidneys from two groups of rats are nearly identical, demonstrating that no agent accumulated in the organs.

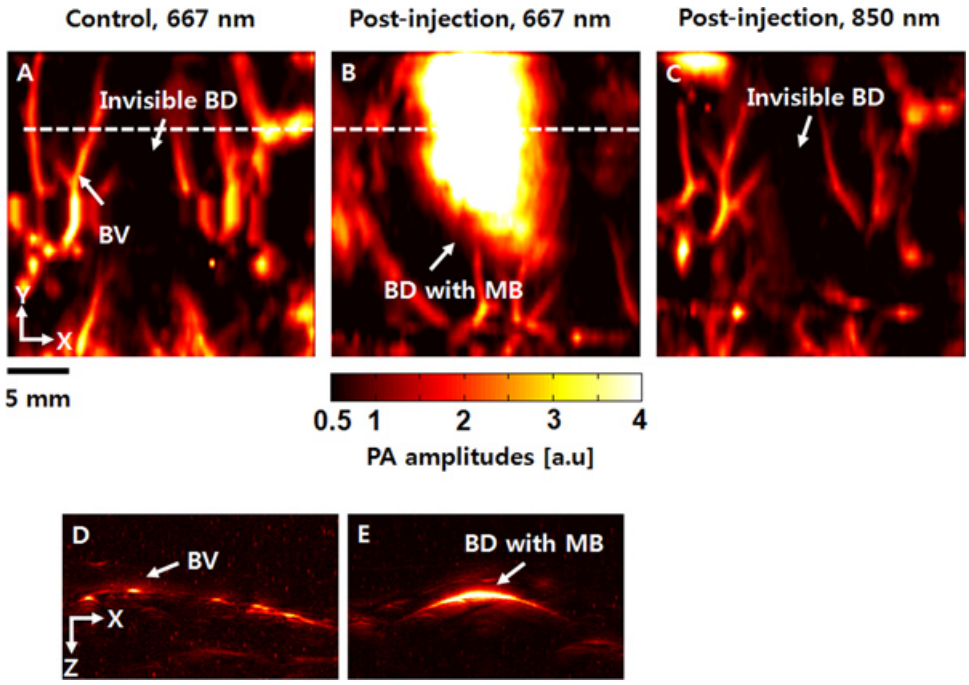

Figure 1. *In vivo* nonionizing and noninvasive PAC using optically opaque methylene blue (MB). (A) Control PA image of a rat's abdominal area acquired at pre-injection of MB with an optical wavelength of 667 nm, showing only blood vessels (BV). This wavelength matches with the optical absorption peak of MB. **(B)** PA image obtained at 0.2 hr post-transurethral-injection of MB with an optical wavelength of 667 nm, revealing both BV and the bladder (BD) accumulated with MB. **(C)** PA image obtained at 850 nm after injection of MB. The BD filled with MB disappears in the PA image because the optical absorption of MB is minimal at this wavelength. **(D)** and **(E)** Depth-resolved PA B-scan images cut along the dotted lines in (A) and (B), respectively. Reprinted with permission from ref [17]. Copyright 2011 Optical Society of America.

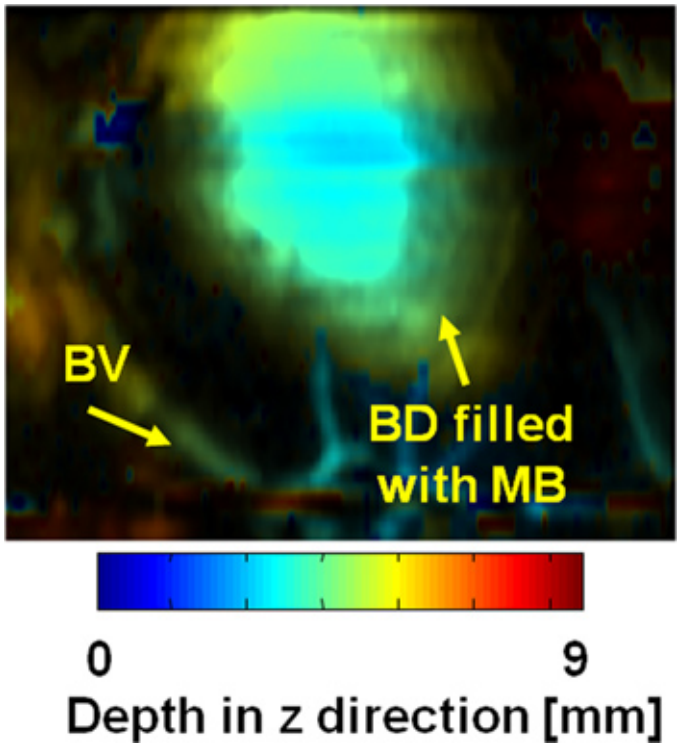

Figure 2. Depth-encoded PA image of Figure 1B. The color represents the depth information. BV, blood vessels; BD, bladder; and MB, methylene blue.

Discussion

In conclusion, we have shown the possibility of nonionizing PAC using nontoxic optical absorbers in a rat model *in vivo*. We have successfully imaged a rat bladder filled with optical absorbents using our nonionizing and noninvasive PAC system. Two critical safety issues have been resolved in our approach: (1) the use of nonionizing radiation for cystographic applications and (2) no accumulation of contrast agents in the body.

Our clinical interest includes monitoring vesicoureteral reflux (VUR) in pediatric patients. About 3% of children in the United States are affected by urinary tract infections[19], and approximately 1.5% of those patients suffer from VUR. In current clinical practice, all these patients directly undergo ionizing X-ray fluoroscopic imaging. The American Urological Association pediatric VUR clinical guidelines panel strongly recommends minimizing the use of ionizing radiation to the pediatric patients.[20] Our long-term goal is to monitor VUR with combination of nontoxic optical contrast agents using PAC. Thus, if there is VUR in patients, we expect that the injected agent will flow back from the bladder to the kidney. Compared with x-ray cystography, PAC has a limited penetration depth. Thus, our main target for clinical PAC is for pediatric patients. Although the imaging speed of our current PAC system is relatively slow due to mechanical scanning, a real-time clinical ultrasound system can be easily adapted for PAC.[21-27] Consequently, this approach potentially offers a portable and inexpensive means to access VUR monitoring, which is an additional benefit. Thus, we strongly believe that the feasibility of clinical translation of our application is very high. For future studies, before it is tested in the clinical setting, the PA VUR monitoring using optical absorbers will be investigated in a porcine model.

Disclosures

All animal experiments were in compliance with the State University of New York at Buffalo Institutional Animal Care and Use Committee.

The authors have nothing to disclose.

Acknowledgements

This work was supported in part by a grant from the pilot studies program of the University at Buffalo Clinical and Translational Research Center and the Buffalo Translational Consortium, a grant from Roswell Park Alliance Foundation, startup funds from the University at Buffalo, IT Consilience Creative Program of MKE, and NIPA (C1515-1121-0003) and NRF grant of MEST (2012-0009249).

References

1. Riccabona, M. Cystography in infants and children: a critical appraisal of the many forms with special regard to voiding cystourethrography. *Eur. Radiol.* **12** (12), 2910-2918 (2002).
2. Khattar, N., Dorairajan, L.N., Kumar, S., Pal, B.C., Elangovan, S., & Nayak, P. Giant obstructive megaureter causing contralateral ureteral obstruction and hydronephrosis: a first-time report. *Urology.* **74** (6), 1306-1308 (2009).
3. Lim, R. Vesicoureteral reflux and urinary tract infection: evolving practices and current controversies in pediatric imaging. *AJR Am. J. Roentgenol.* **192** (5), 1197-1208 (2009).
4. Scardapane, A., Pagliarulo, V., Ianora, A.A., Pagliarulo, A., & Angelelli, G. Contrast-enhanced multislice pneumo-CT-cystography in the evaluation of urinary bladder neoplasms. *Eur. J. Radiol.* **66** (2), 246-252 (2008).
5. Verpoorten, C. & Buyse, G.M. The neurogenic bladder: medical treatment. *Pediatr. Nephrol.* **23** (5), 717-725 (2008).
6. Ron, E. Let's not relive the past: a review of cancer risk after diagnostic or therapeutic irradiation. *Pediatr. Radiol.* **32** (10), 739-744 (2002).
7. Berrington De Gonzalez, A. & Darby, S. Risk of cancer from diagnostic X-rays: estimates for the UK and 14 other countries. *Lancet.* **363** (9406), 345-351 (2004).
8. Kim, C., Favazza, C., & Wang, L.V. *In vivo* photoacoustic tomography of chemicals: high-resolution functional and molecular optical imaging at new depths. *Chem. Rev.* **110** (5), 2756-2782 (2010).
9. Ke, H., Erpelding, T.N., Jankovic, L., Liu, C., & Wang, L.V. Performance characterization of an integrated ultrasound, photoacoustic, and thermoacoustic imaging system. *J. Biomed. Opt.* **17** (5), 056010 (2012).
10. Akers, W.J., Kim, C., Berezin., *et al.* Noninvasive Photoacoustic and Fluorescence Sentinel Lymph Node Identification using Dye-Loaded Perfluorocarbon Nanoparticles. *Acs Nano.* **5** (1), 173-182 (2011).
11. Jiao, S.L., Jiang, M.S., Hu, J., *et al.* Photoacoustic ophthalmoscopy for *in vivo* retinal imaging. *Opt. Express.* **18** (4), 3967-3972 (2010).
12. Kim, C., Cho, E.C., Chen., J., *et al. In vivo* molecular photoacoustic tomography of melanomas targeted by bioconjugated gold nanocages. *Acs Nano.* **4** (8), 4559-4564 (2010).
13. Kim, C., Song, H.M., Cai, X., Yao, J., Wei, A., & Wang, LV. *In vivo* photoacoustic mapping of lymphatic systems with plasmon-resonant nanostars. *J. Mater. Chem.* **21** (9), 2841-2844 (2011).
14. Wang, X., Pang, Y., Ku, G., Xie, X., Stoica, G., & Wang, L.V. Noninvasive laser-induced photoacoustic tomography for structural and functional *in vivo* imaging of the brain. *Nat. Biotechnol.* **21** (7), 803-806 (2003).
15. Xie, Z., Roberts, W., Carson, P., Liu, X., Tao, C., & Wang, X. Evaluation of bladder microvasculature with high-resolution photoacoustic imaging. *Opt. Lett.* **36** (24), 4815-4817 (2011).
16. Zhang, H.F., Maslov, K., Stoica, G., & Wang, L.V. Functional photoacoustic microscopy for high-resolution and noninvasive *in vivo* imaging. *Nat. Biotechnol.* **24** (7), 848-851 (2006).
17. Kim, C., Jeon, M., & Wang, L.V. Nonionizing photoacoustic cystography *in vivo*. *Opt. Lett.* **36** (18), 3599-3601 (2011).
18. Homan, K., Kim, S., Chen, Y.S., Wang, B., Mallidi, S., & Emelianov, S. Prospects of molecular photoacoustic imaging at 1064 nm wavelength. *Opt. Lett.* **35** (15), 2663-2665 (2010).
19. Chang, S.L. & Shortliffe, L.D. Pediatric urinary tract infections. *Pediatr. Clin. N. Am.* **53** (3), 379 (2006).
20. Stratton, K.L., Pope, J.C., Adams, M.C., Brock, J.W., & Thomas, J.C. Implications of Ionizing Radiation in the Pediatric Urology Patient. *J. Urology.* **183** (6), 2137-2142 (2010).
21. Ermilov, S.A., Khamapirad, T., Conjusteau, A., *et al.* Laser optoacoustic imaging system for detection of breast cancer. *J. Biomed. Opt.* **14** (2), 024007 (2009).
22. Erpelding, T.N., Kim, C., Pramanik, M., *et al.* Sentinel lymph nodes in the rat: noninvasive photoacoustic and US imaging with a clinical US system. *Radiology.* **256** (1), 102-110 (2010).
23. Kim, C., Erpelding, T.N., Jankovic, L., & Wang, L.V. Performance benchmarks of an array-based hand-held photoacoustic probe adapted from a clinical ultrasound system for non-invasive sentinel lymph node imaging. *Philos. Transact. A. Math Phys. Eng. Sci.* **369** (1955), 4644-4650 (2011).
24. Kim, C., Song, K.H., Gao, F., & Wang, L.V. Sentinel lymph nodes and lymphatic vessels: noninvasive dual-modality *in vivo* mapping by using indocyanine green in rats--volumetric spectroscopic photoacoustic imaging and planar fluorescence imaging. *Radiology.* **255** (2), 442-450 (2010).
25. Kruger, R.A., Kiser, W.L., Reinecke, D.R., & Kruger, G.A. Thermoacoustic computed tomography using a conventional linear transducer array. *Medical Physics.* **30** (5), 856-860 (2003).
26. Kruger, R.A., Lam, R.B., Reinecke, D.R., Del Rio, S.P., & Doyle, R.P. Photoacoustic angiography of the breast. *Med. Phys.* **37** (11), 6096-6100 (2010).
27. Manohar, S., Kharine, A., Van Hespen, J.C., Steenbergen, W., & Van Leeuwen, T.G. The Twente Photoacoustic Mammoscope: system overview and performance. *Phys. Med. Biol.* **50** (11), 2543-2557 (2005).

